
Article:
Shah, M.Q., Murtaza, G., Shafiq, M. et al. (2 more authors) (2023) Investigation of optoelectronic & thermoelectric features of ZnCrX2 (X= S Se Te) chalcopyrite semiconductor using mBJ potential. Chinese Journal of Physics, 85. pp. 1-14. ISSN 0577-9073

https://doi.org/10.1016/j.cjph.2023.05.016

Investigation of optoelectronic & thermoelectric features of $ZnCrX_2$ (X= S Se Te) chalcopyrite semiconductor using mBJ potential

M. Qasim Shah[a*], G. Murtaza[b**], Maleeha Shafiq[b], S. Sharif[c], Nicola A. Morley[d]

[a]Department of Electrical Engineering, University of the Punjab, Lahore-Pakistan
[b]Centre for Advanced Studies in Physics, GC University, Lahore 54000, Pakistan
[c]Department of Physics, GC University, Lahore 54000, Pakistan
[d]Department of Materials Science and Engineering, The University of Sheffield, S1 3JD, UK

Abstract

In the present investigation, we have examined the structural, optoelectronic and thermoelectric properties of the compound $ZnCrX_2$ (X=S, Se, Te) using the full potential linearized augmented plane wave (FP-LAPW) method with the generalized gradient approximation (GGA-PBE) and the modified Becke–Johnson (mBJ) implemented on Wien2k code. By calculating the electronic structure, we observed that the indirect band gap was 1.76 eV, 1.68 eV, and 1.59 eV, for these selected compounds and the type of chemical bonding was ionic between Zn-X and Cr-X. For the three ternary chalcopyrites their optical properties including optical conductivity, complex dielectric functions, complex refractive index, reflectivity, energy loss, and absorption coefficient were examined. The calculated optical conductivity indicates that the studied compounds are suitable for optoelectronic applications as they have good absorbance and less energy loss in the a low energy range of the electromagnetic spectrum. For ZnCrTe2, the maximum reflectivity was in the low energy range (0.48 or 48% at 9 eV). The BoltzTrap code was executed for the calculation of the thermoelectric properties and thermal efficiency of the compounds investigated, depending upon the Seebeck coefficient, thermal conductivity and electrical conductivity. The high value of the figure of merit and the Seebeck coefficient (260 uV/k) defines the high efficiency of the materials studied. Hence, the studied chalcopyrite compounds offer applications in solar cell devices and p-type semiconducting nature predictive in transport investigations.

Keywords:

Semiconductor; Modified Becke Johnson potential; Optoelectronic application; Thermoelectric properties

Corresponding author E-mail: qasimshah1997@gmail.com*, gmrai@gcu.edu.pk**

1. Introduction:

With the exponential growth of the world population and the extending use of modern electronic devices, it is impossible to keep up with the ever-increasing energy demand. Recently, solar panels have seen an improvement in their efficiency, which has been depicted in recent trends [1]. The vast majority of commercially available solar products are built using silicon-based technology. The development of affordable solar cell materials with greater efficiency is a growing area at the present [2], [3]. However, by employing certain techniques, it is possible to improve the yield of solar energy, despite the challenges that this proposes [1], [4].

Chalcopyrite type semiconductors are considered important in the context of solar cell optoelectronic technology. The main rationale for their use is the upgrading of the capability and the functionality in different applications, which may include: Solar Cells, Light Emitting Diodes, filters used in nonlinear optics, and photovoltaic detectors [5]. The formula for chalcopyrite compounds is $A^{I}B^{III}C_2$ which is known as ternary chalcopyrite compounds [6]. Their other general family groups include $CuXY_2$ (Y=S, Se and X=In, Ga) [7], $AgGaSe_2$ [8], $AgTiX_2$ (X = S, Se, Te) [9] and $AgAlM_2$ (M=S, Se, Te) [10] having a direct band gap, which ranges from 1.4 eV to 3.05 eV. The properties of chalcopyrite material suggest that they may be important in the absorption, and evolution of certain visible ranges of the solar spectrum [11]. Kushwaha et al. studied the phonon and elastic properties of $ABSe_2$ (A = Cu and Ag; B = Al, Ga and In) materials for solar cell applications [12]. Transition-metals based chalcopyrite s are specific types of earth materials that include the following properties: catalytic , various electronic, optical, and magnetic [13]. Using first-principles calculations, Ranjan et al., have introduced Ag-based chalcopyrite having formula $AgTiX_2$ (X = S, Se, Te). They studied and gained the experimental results, which showed a rectangular geometry, having a maximum highest occupied molecular orbital and lowest occupied molecular orbital (HOMO-LUMO) gap as well as doublet spin multiplicity associated with certain $AgTiS_2$ compound [9]**.** Electronic and Structural properties were examined by Ranjan et al., and they calculated the HOMO-LUMO energy gap for the compound $CuTiX_2$ (X = S, Se and Te) to have a range of energy gaps between 2.405 to 3.197 eV **[5]**. The study of $ZnMnO_2$ chalcopyrite and $ZnCrO_2$

has been done by Tabti et al., using TB-mBJ potential and reported wide band gaps in the spin-down channel [14].

This work aims to investigate the optical and thermoelectric behavior of a series of ternary chalcopyrites $ZnCrX_2$ (X = S, Se, Te) exhibiting body-centered tetragonal structure in the *I-42d* phase [15,16]. To check the electronic behavior of chalcopyrite compounds mBJ potential wa s employed since GGA approximation yields an underestimated band gap value. Moreover, the BoltzTrap code was used to calculate the thermoelectric properties of the studied compounds.

2. Computational details:

Density Functional Theory (DFT) formalism was employed by (FP-LAPW) [17-18] scheme in Wien2k code [19] for the study of $ZnCrX_2$ (X=S, Se, Te) chalcopyrite. Perdew Burke Ernzerhof Generalized Gradient Approximation (PBE-GGA) [20] and modified Becke Johnson method (mBJ) approach [21] we re adopted for exchange correlation potential. By considering a cut-off of $R_{mt}K_{max}$ = 9.0, the wave functions plane was enlarged in a zone known as the interstitial zone. The value of the potential and G_{max}=12 shows the Fourier charge density has increased, while the spherical harmonic functions have a value l_{max}=10. The total is converged without even overlapping the atomic spheres −9.0 Ry and it's cut-off energy, which calculates the segregation with the valence states and the core. 1000 k-points (10 × 10 × 10) were used for the betterment of the energy convergence within the Monk Horst-Pack k-mesh test [22]. The self-consistent field for the convergence criteria of energy was set to the values of 10^{-5} Ry, 10^{-4} e for energy and charge respectively**.** We used the modified Becke-Johnson type potential, which is an accurate recent potential to calculate the band gap value [23], resulting in a better, more accurate band structure computation that is similar to the experimental data. The following relation was used for the calculation in DFT

$$u_{x,\sigma}^{mBj}(r^{\rightarrow}) = cu_{x,\sigma}^{BR} + (3c-2)\frac{1}{\pi}\sqrt{\frac{5}{6}\sqrt{\frac{\tau_\sigma(r^{\rightarrow})}{\rho_\sigma(r^{\rightarrow})}}} \qquad (1)$$

Where $u_{x,\sigma}^{BR}$ is the Becke-Roussel potential, ρ_σ represents the symbol for electron density, τ_σ resembles (K.E) kinetic energy, [24] parameter c defines the System-Dependent parameters, where in equation 1, c=1 corresponds to the actual Becke-Johnson potential. For bulk

crystalline materials, an empirical relation was introduced by Blaha and Tran for the calculation of C (equation 2), which is: :

$$C = \alpha+\beta\left(\frac{1}{V_{cell}} \int_{cell} \frac{\nabla\rho_{\sigma}(r')}{\rho_{\sigma}(r')} d^3r'\right)^{\frac{1}{2}} \quad (2)$$

Where the unit cell volume (V_{cell}), α and β values −0.012 & 1.023 $bohr^{1/2}$ respectively are determined from the crystal structure as seen in Fig 1 [25, 26].

3. Results & details

3.1 Structural details:

3.1.1: Geometry of unit cell:

The ternary chalcopyrite compound crystallizes with a body centered tetragonal structure [27] at absolute pressure and temperature. The I-42d space group unit cell consists of 8 positions, which have been elaborated in Fig. 1. Within the computation, the corresponding atoms positions within a unit cell of chalcopyrite structure have been employed : Zn (0, 0,0) (0, 1/2, 1/4); Cr (1/2, 1/2, 1/2) (0, 1/2, 3/4); S/Se/Te (μ, 1/2, 1/8) (–μ, 3/4, 1/8) (3/4, μ, 7/8), and (1/4, –μ, 7/8). To obtain the minimized energy of the unit cell for the compounds $ZnCrX_2$ (X= S, Se and Te), for the approximate optimization of the lattice parameters, GGA-PBE has been adopted. The unit cell optimized calculations are done for the lattice parameters a, (c/a), (B_0) the bulk modulus, and the pressure derivative of the first bulk modulus (B'). Murnaghan's equation of state [28] is used for the calculation of the total energy from which the ground state energy and volumes are determined. $\left[B' \left(1 - \frac{V_O}{V}\right) - \left(\frac{V_O}{V}\right)^3 - 1\right]$ The energy versus volume fitting curve has been presented in Fig. 2, which represents the ground state energy of the concerning compounds. After optimization the calculated lattice parameters, including *a*, *c*, *η*, B_0 in GPa, bulk modulus derivative B' in GPa, the ground state energy E_0 and Volume V_0 *are presented* in Table 1. It is observed that by replacing the atoms as S →Se →Te in the compound $ZnCrX_2$, the lattice constants *a, c,* volume, and ground state energy increases but the pressure bulk modulus and its derivative decreases. For an ideal case, the tetragonal chalcopyrite structure has bond lengths which are equal, $\eta = \frac{c}{2a} = 1$ **.** As **η**≠ 1 , this means that there is distortion within the ideal tetragonal structure and anion displacement is present [29]. A measure of distortion in the unit cell bond lengths can be calculated.

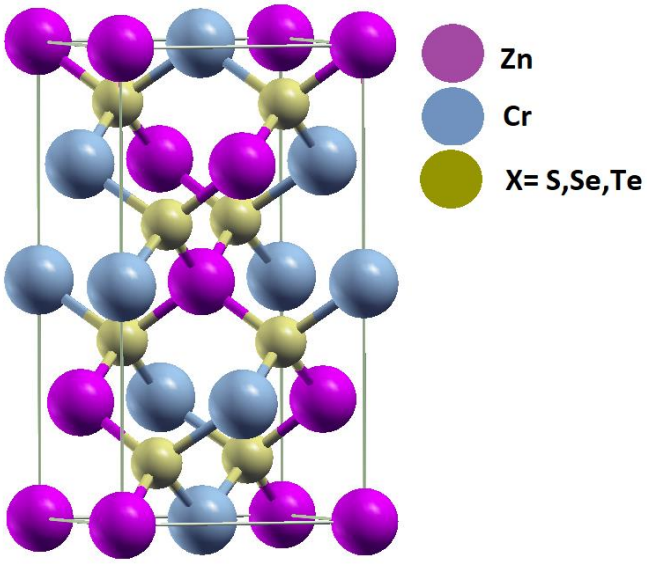

Fig. 1. Crystal Structure of $ZnCrX_2$ (X= S, Se, Te) chalcopyrite compounds using PBE-GGA

3.1.2 Bond length:

The crystal lattice of the chalcopyrite structure is indicated by the lattice parameters *a*, *c,* bond length (R_{Zn-X}, R_{Cr-X}) and dimensionless anionic displacement *u* which is known as the internal parameter [30]. Anion displacement *u* represents how an anion displaces from its ideal position in a tetrahedron. The bond length of two chemical bonds (*Zn–X and Cr–X)* was determined using equations 3 and 4, [31]:

$$R_{Zn-X} = a[u^2 + \frac{1+\eta^2}{16}]^{\frac{1}{2}} \quad (3)$$

$$R_{Cr-X} = a[\left(u^2 - \frac{1}{2}\right)^2 + \frac{1+\eta^2}{16}]^{\frac{1}{2}} \quad (4)$$

From the ideal case, the internal parameter *u* = 0.25, but for the non-ideal case, the bond length is $R_{Zn-X} \neq R_{Cr-X}$ due to dissimilar atoms in $ZnCrX_2$ (X= S, Se, Te**)**, thus *u* ≠ 0.25. In the case where the calculated parameters are larger than the ideal parameter, tetragonal anion distortion is higher [32]. The question arises, how much alteration occurs in the bond of a system? The answer to this, is determined by anion displacement *u* and calculated by using the relation:

$$u = 0.25 + (\frac{R_{Zn-X}^2 - R_{Cr-X}^2}{a^2}) \quad (5)$$

Bond length **(R_{Zn-X}, R_{Cr-X})** and anion displacement *u* are presented in Table:1**.** For $ZnCrX_2$ compounds, the range from 0.347 to 0.375 shows the anion displacement *u* which further leads towards distortion from ideal Zinc blend structure known as small tetragonal distortion. Whereas we discuss the representation values, when *u* is less than 0.25 ($u < 0.25$), the Cr site anion X is displaced away from it, hence showing the movement toward the Zn site, which results in a shorter bond length of Zn–X as compared to the Cr–X bond length, which overall results towards volume compression. When *u* is greater than 0.25 ($u > 0.25$), then the anion X shows the movement towards the Cr site, which results in the increment of Zn–X bond length. Thus the overall result leads towards expanded volume [33]. It can be seen from Table 1 that $u > 0.25$, then there is a shorter Cr-X bond length and an increase in bond length of Zn–X that further leads towards volume expansion. The value of the bond lengths increases by replacing atoms, as S →Se →Te anion displacement is increasing and volume is also increasing**.**

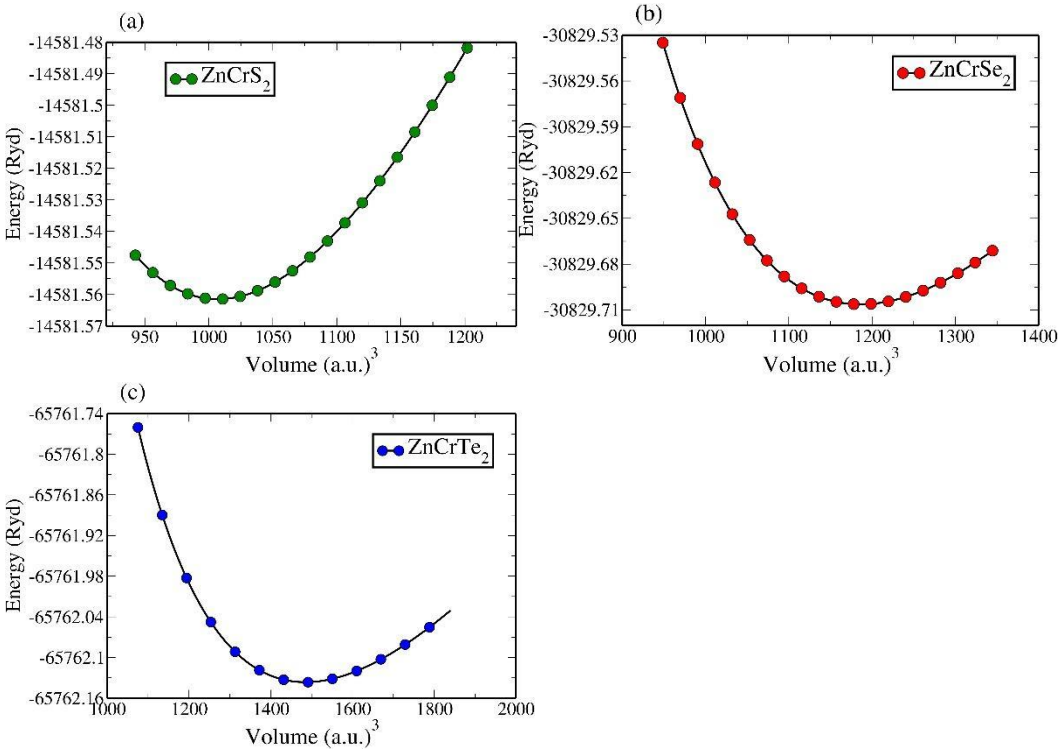

Fig. 2. Total energy Vs volume curves of $ZnCrX_2$ (X= S Se Te) using PBE-GGA approximation

Table 1: Lattice constants (a & c), pressure bulk modulus and its derivative, ground state energy and volume, internal parameters (η and u), and bond length.

Compound	*a=b* (Å)	*c* (Å)	B_0 GPa	B' GPa	$E_\circ$ (Ryd)	$V_\circ$ $(a.u.)^3$	$\eta=\frac{c}{2a}$ -	R_{Zn-X} (Å)	R_{Cr-X} (Å)	*u* -
$ZnCrS_2$	5.71	10.67	88.405	5	-14581.561	1007.075	0.934	2.447	1.672	0.347
$ZnCrSe_2$	5.87	11.25	64.022	5	-30829.706	1185.716	0.958	2.5818	1.7708	0.352
$ZnCrTe_2$	6.62	11.95	53.699	4.5	-65762.136	1483.516	0.902	2.992	1.8579	0.375

3.2 Electronic properties:

It is important to understand the electronic behavior of materials as it helps us gain an appropriate domain for their use and the results lead us to confirm the demand for material specially in the solar cell field [34]. The band structure and the state densities using the mBJ potential have been plotted in Fig. 3.

2.2.1 Band Structure:

The band structure curves of these compounds were studied and show the representation of the conduction band and valence band having a Fermi level within the energy gap between the bands The indirect band gap values are estimated by using TB-mBJ approximation, the calculated values are 1.76 eV, 1.62 eV and 1.59 eV for $ZnCrS_2$, $ZnCrSe_2$ and $ZnCrTe_2$ respectively. Hence this shows that the behavior of these three compounds is semiconductor behavior. A decrease in band gap is found with the transition of atom from S to Te in the $ZnCrX_2$ compound. An analogous decrease within the band gap of these materials $ZnCrX_2$ (X=S, Se, Te) results in the anions substitution of S, Se, and Te and this behavior is reported in other theoretical articles [35]. Hence it is concluded that by decreasing the band go to 1.59 eV, the anions S, Se, & Te have played a vital role. Similarly, the semiconductor nature and smaller band gaps confirm that the concerning materials are good candidates for the production of photovoltaic gadgets.

3.2.2 Total & Partial Density of States (TDOS and PDOS):

The density of states plays a major role and provides a vital tool in the disclosure of the physical properties of any material. This investigation leads us to know the involvement of atomic states to a specific band set by decomposing the (TDOS) total density of states into the orbital contributions (s, p, and d), that describe the projected density of states (PDOS) [36]. Therefore, it strengthens for explaining the general characteristics of bonding within such materials which are shown in Figure 3. This figure shows the results regarding the partial and total electronic density of states. Gaps within the states of the conduction band and the valence band in the total density of states confirm the semiconducting behavior of the compounds.

For all three compounds, the Cr-d and S/Se/Te-p orbitals are mainly driven by the electronic states around the valence band ranges from -2 eV to -3 eV, whereas the Cr-d states dominate in conduction band ranges from about 2 eV to 3 eV. We remark that nearly all of the S/Se/Te p-states are in the middle within the valence band from -3 eV to -5 eV, while negligible contribution is present in the conduction band. Whereas, the Cr-d character and its presence within the upper valence band (0 to -0.5 eV) plays an important role in the optical band gaps within these materials [37].

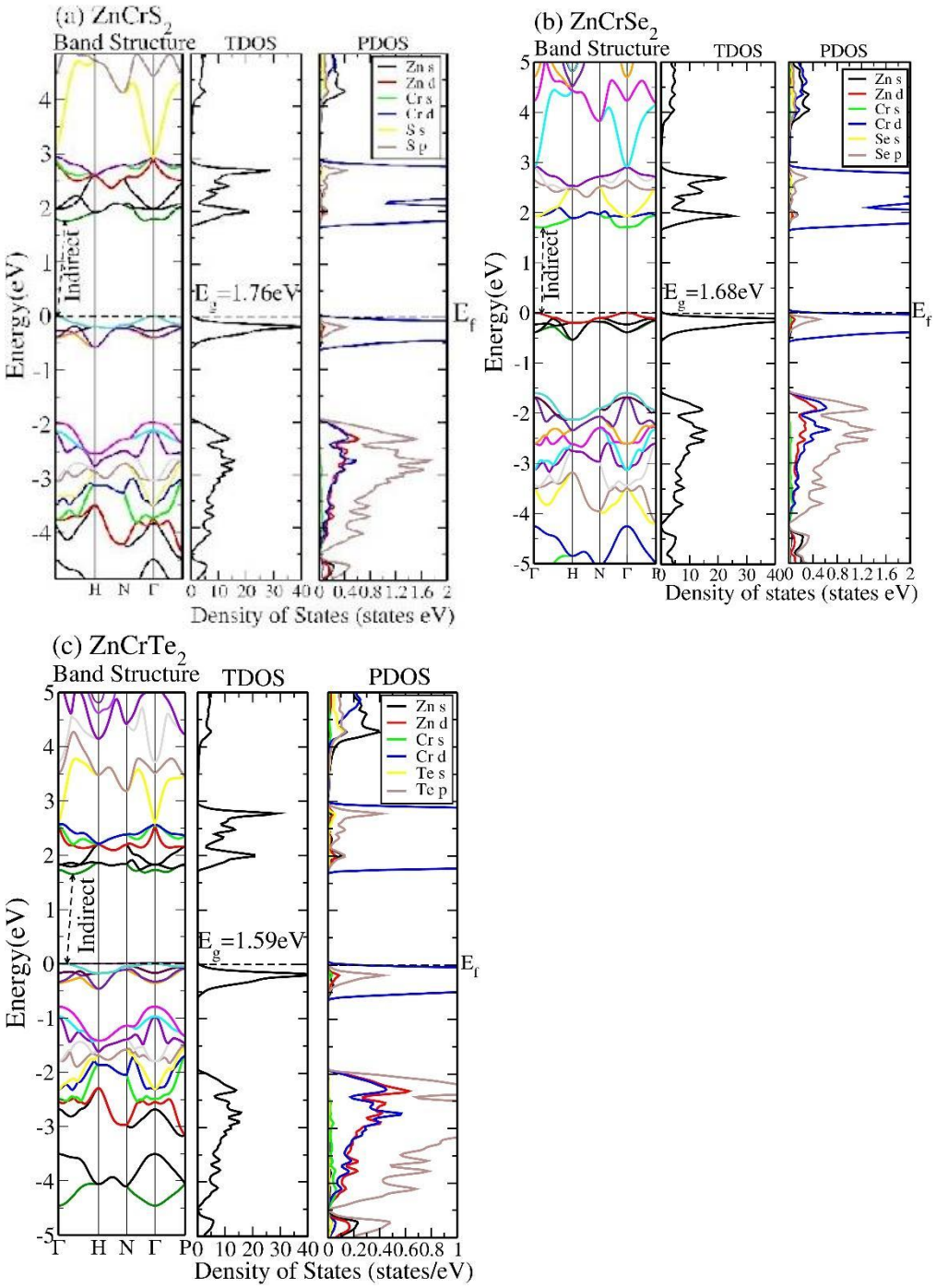

Fig. 3. Total densities of states (TDOS) & band structure of $ZnCrX_2$ compounds:(a) $ZnCrS_2$, (b) $ZnCrSe_2$ (c) $ZnCrTe_2$ using mBJ potential

3.3.2 Electronic Charge Density:

The chemical bonding present within the elements of the ternary chalcopyrite ZnCrX2 (X=S, Se, and Te) compounds depends on the band structure as well as the density of states (DOS), , thus we need to calculate the electronic charge density within the (100) plane, with mBJ potential as shown in Fig. 4(a-c). When the electronegativity difference is large the ionic bond occurs whereas the covalent bond occurs with a small electronegativity difference [38]. We observed that when the Zn, Cr, S, Se, and Te charge is transferred, their results show an ionic bond nature, this is caused due to a huge difference within the electronegativity present between them. These electronegativity values for Zn, Cr, S, Se, and Te are 1.65, 1.66, 2.58, 2.55, and 2.1 respectively. The electronegativity difference Zn and Cr with S is (0.93 and 0.92), with Se is (0.9 and 0.89) and with Te is (0.45 and 0.44), observed that ionic bond character is decreasing by replacing the S atom with Se and Te. Fig. 4 (a-c) shows the spherical representation for the charge density lines among the atoms, and the figure also indicates the ionic bonding of the examined components.

(a) $ZnCrS_2$ (b) $ZnCrSe_2$ (c) $ZnCrTe_2$

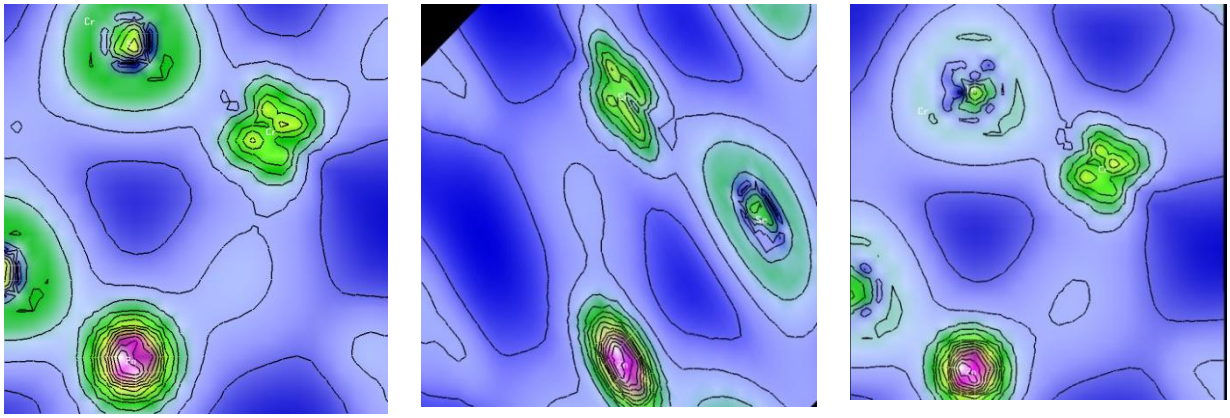

Fig.4. Electronic Charge Density (ECD) representation of (a) $ZnCrS_2$ (b) $ZnCrSe_2$ (c) $ZnCrTe_2$ compounds using mBJ potential

3.3 Optical properties:

In the discussion of optical properties, the optical response of material can be acquired from the Complex Dielectric Function (CDF) which is related to the band structure [39].

3.3.1 Complex Dielectric Function (CDF):

The CDF is determined by using Maxwell's equations. The presence of the electromagnetic wave CDF mainly attributes to the inter-band transition, which is beneficial for the formation of semiconductors and the intra-band transition, which is useful for the formation of metals [40]. The optical properties of the concerning compound are examined which elaborates on the linear optical properties present in materials. The formalism for complex dielectric function depending on Ehrenreich Cohen is given [41,42]: $\boldsymbol{\varepsilon(\omega) = \varepsilon_1(\omega) + i\varepsilon_2(\omega)}$

The dielectric function is divided into two parts:

1. Real part $\varepsilon_1(\omega)$
2. Imaginary part $\varepsilon_2(\omega)$

The second part (imaginary part) gives us the representation of how much energy is absorbed by the material, it is stated as follows [43]:

$$\varepsilon_2(\omega) = \frac{4\pi^2 e^2}{m^2\omega^2}\sum_{ij} \quad i|M|j^2 f_i(1-f_i)\delta(E_f - E_i - \omega)d^3k \qquad (6)$$

A photon incident on the material means that dispersion occurs that is presented by the real part of dielectric $\varepsilon_1(\omega)$. By using the Kramer's Kronig relation [44] it can be obtained from the matrix of the imaginary part of dielectric $\varepsilon_2(\omega)$.

$$\varepsilon_1(\omega) = 1 + \frac{2}{\pi}P\int_0^\infty \quad \frac{\omega'\varepsilon_2(\omega')}{\omega'^2-\omega^2}d\omega' \qquad (7)$$

In Fig. 5(a, b) the results of the dielectric function $\varepsilon_1(\omega)$ and $\varepsilon_2(\omega)$ are calculated for both the real and imaginary parts, with the function energy ranging from 0 to 12 eV. $\varepsilon_1(\omega)$ gives the representation about how much dispersion by the incident photon within the material, and $\varepsilon_2(\omega)$ resembles how much energy is absorbed by the material [45]. $\varepsilon_2(\omega)$ is also related to the optical transitions between the conduction band and the valence band, which give confirmation of the band gap for the concerning compounds $ZnCrX_2$(X= S, Se, Te) with the result is obtained in the band structure [46].

Fig. 5a displays the calculated real part values as a function of incident photon energy. At zero frequency, the real part of the dielectric is called a static optical dielectric constant. Band gap variations are described by a static dielectric constant depending on the Kronig-Penney model [44]. The compounds which have shorter band gaps possess higher static dielectric constant

values [47]. The static dielectric functional $\varepsilon_1(0)$ values are 4.9, 5.6, and 6.5 for $ZnCrX_2$ (X= S, Se, Te) and it is highest for $ZnCrTe_2$ while the band gap is smallest . Also, $ZnCrS_2$ has a smaller dielectric function $\varepsilon_1(0)$ while the band gap is larger. The studied materials show the value of $\varepsilon_1(\omega)$ has greater values in the range (3–5 eV) representing maximum polarization and minimum dispersion of light from the material [47]. Hence it is observed that the real part of the dielectric function $\varepsilon_1(\omega)$ increases until reaching a maximum showing major peaks at 4.5 eV, 4.1 eV, and 3.2 eV for $ZnCrS_2$, $ZnCrSe_2$, $ZnCrTe_2$ respectively, with the peaks shifting to lower energy values from S to Te. Then the $\varepsilon_1(\omega)$ decrease to the negative values for the three studied compounds. The incident photons are entirely reflected because the real part of the dielectric constants has a negative value and the compound shows metallic behavior in this region [48]. In Fig. 5b; the imaginary part of dielectric $\varepsilon_2(\omega)$ shows that the threshold values of concerning compounds are 1.3 eV, 1.2 eV and 1.1 eV, which show the start of optical transition in compounds. Also, the peaks of the imaginary parts of the dielectric constant $\varepsilon_2(\omega)$ reach their maxima at 5 eV, 4.5 eV and 3.5 eV for $ZnCrS_2$, $ZnCrSe_2$ and $ZnCrTe_2$ respectively. The large size of the peaks can be explained by an important absorption of the phonons [11]. It is found that $ZnCrTe_2$ exhibits higher absorption in comparison to $ZnCrS_2$ and $ZnCrSe_2$ compounds with higher energy photons.

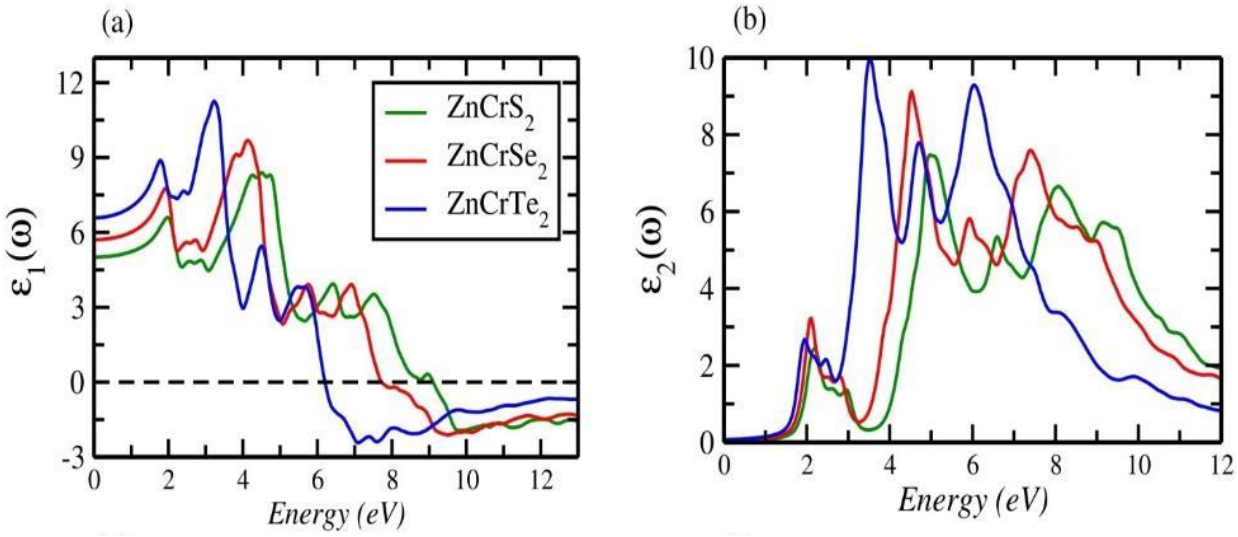

Fig. 5. Dielectric function (a) Real part $\varepsilon_1(\omega)$. (b) Imaginary part $\varepsilon_2(\omega)$ of $ZnCrX_2$ (X= S Se Te) as a function of photon energy using mBJ potential

3.3.2 Complex Refractive Index:

The complex refractive index, ˜n = n + ik, with *n* as the phase velocity and *k* as the extinction coefficient was calculated according to the following relations: $n^2 - k^2 = \varepsilon_1(\omega)$ real part and $2nk = \varepsilon_2(\omega)$ the imaginary part of the complex refractive index [49].

The refractive index is a dimensionless number that describes the propagation of light through material and the values elucidate different spectroscopic data [23], [50]. The refractive index measures the transparency of a material [51] and by using dielectric functions formulated as: $n(\omega) = \sqrt{\frac{\sqrt{\varepsilon_2^2(\omega)+\varepsilon_1^2}(\omega)+\varepsilon_1(\omega)}{2}}$. In Fig. 6a, the results show that the static refractive index *n*(0) (refractive index at zero frequency) value is 2.2, 2.3, and 2.5 for $ZnCrS_2$, $ZnCrSe_2$, and $ZnCrTe_2$ respectively. It was found that it is related to the real part of dielectric function by the relation: $n(0) = \sqrt{\varepsilon_1(0)}$ [52]. The increase in energy shows the increase in the refractive index values, with a few sharp peaks in the energy range of 3–5 eV, which implies these materials are applicable for optoelectronic devices [53]. The highest refractive index value is determined around 4.8 eV, 4.2 eV, and 3.3 eV for $ZnCrS_2$, $ZnCrSe_2$, and $ZnCrTe_2$ respectively. Thus, $ZnCrTe_2$ has the highest refraction among these materials with maximum transparency. The refractive index decreases to its minimum value of around 12.0 eV as interacting photons increase. If the refractive index is less than 1, then phase velocity increases but the group velocity remains less than the speed of light, thus the equation of relativity remains unaffected [38].

The extinction coefficient is the decay or damping in the oscillation amplitude of the incident electric field [54]. The extinction coefficient based on the dielectric function is determined by the relation [55]: $n(\omega) = \sqrt{\frac{\sqrt{\varepsilon_2^2(\omega)+\varepsilon_1^2}(\omega)-\varepsilon_1(\omega)}{2}}$. It reveals the capability of the material to absorb incident light and is similar to $\varepsilon_2(\omega)$ [51]. The extinction coefficient *K*(ω) is presented in Fig. 6b and it shows that $ZnCrSe_2$ has a greater value than $ZnCrS_2$ and $ZnCrTe_2$ in the visible region of the electromagnetic spectrum. While $ZnCrTe_2$ has a greater value for high energy photons in the ultraviolet region ranging from 3 eV to 7 eV, then decreases to a lower extinction coefficient after 8 eV of photon energy.

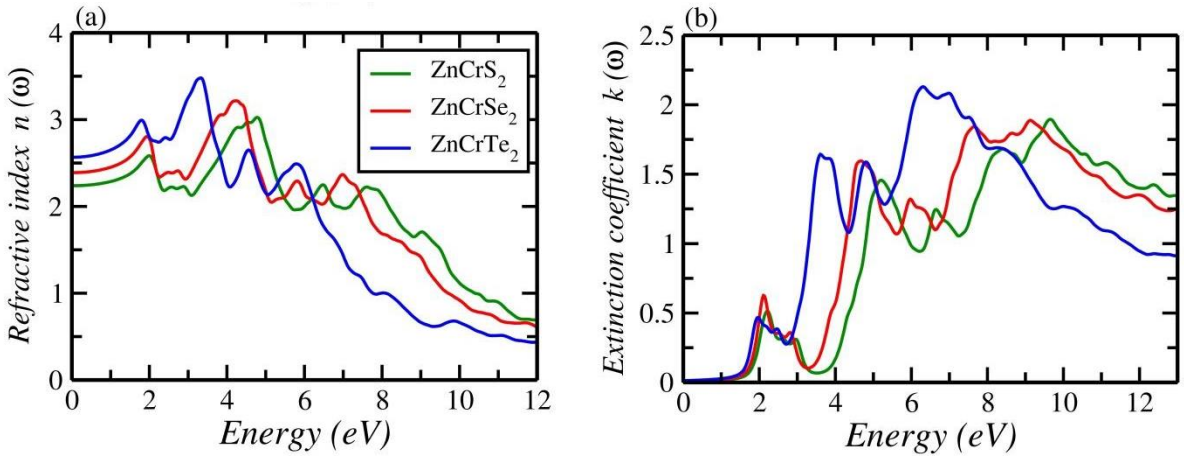

Fig. 6. **(a)** Refractive index n(ω) and **(b)** extinction coefficient $K(\omega)$ as a function of the photon energy of compounds ZnCrX2 (X= S Se Te) using mBJ potential.

3.3.3 Optical conductivity and absorbance coefficient:

Optical conductivity $\sigma(\omega)$ studies the conduction process that emerges from a photo electron that interacts with a material Fig. 7 (a) shows the optical conductivity calculated by the relation: $\sigma(\omega) = \frac{\omega}{4\pi}\varepsilon_2(\omega)$ [56] and it provides information about the optical transitions of the materials. Higher optical conductivity of all compounds were found in the 6–8 eV range and the sharp peaks are shifted to lower photon energy by changing the atoms in order of S →Se →Te at 8.1 eV, 7.4 eV, and 6.1 eV values respectively. It was found that $ZnCrTe_2$ has greater optical conductivity for low energy photons, this is indicative of large absorption of a photon in this range. These materials exhibit significant absorption in the UV region of the solar spectrum, making them ideal for UV detectors, X-ray phosphors, photovoltaic materials for space technologies, and LED solid-state illumination [57].

The absorption coefficient shows how much light an electromagnetic wave loses when it travels through a material of a given thickness [58] and the absorption coefficient can be calculated as [59]: $\alpha(\omega) = \frac{\sqrt{2}\omega}{c}\sqrt{\sqrt{\epsilon_1^2(\omega)+\epsilon_2^2(\omega)} - \epsilon_1(\omega)}$. Fig. 7(b) shows the absorbance coefficient perpendicular to c of the electromagnetic waves up to 12 eV, for the different compounds. It is observed that the materials can absorb incident photons through direct and indirect electronic transitions, when the energy of the incident solar radiation exceeds the energy band gap (E_g) of the material. The fluctuation in the absorption edge of $ZnCrS_2$, $ZnCrSe_2$, $ZnCrTe_2$ at 1.8 eV, 1.7 eV and 1.6 eV is related to the band gap, which begins at approximately

the same value of $\varepsilon_2(\omega)$. Also, maximum absorption is in the ultraviolet region with the greatest values for $ZnCrS_2$ and $ZnCrSe_2$ in the range of 9-12 eV, while it decreases for $ZnCrTe_2$ in this region. The greater optical conductivity and absorbance of $ZnCrTe_2$ is in the range from 3 eV to 7 eV. It is found that results correspond with the other chalcopyrite compounds like $NaGaS_2$, $NaGaSe_2$, $NaGaTe_2$, $GaCuS_2$, $InCuS_2$, and $AlCuS_2$ in the photon energy range of 6–10 eV [60,11]. From the absorption edge values it can be concluded that the $ZnCrX_2$ compounds are good candidates for optoelectronic devices.

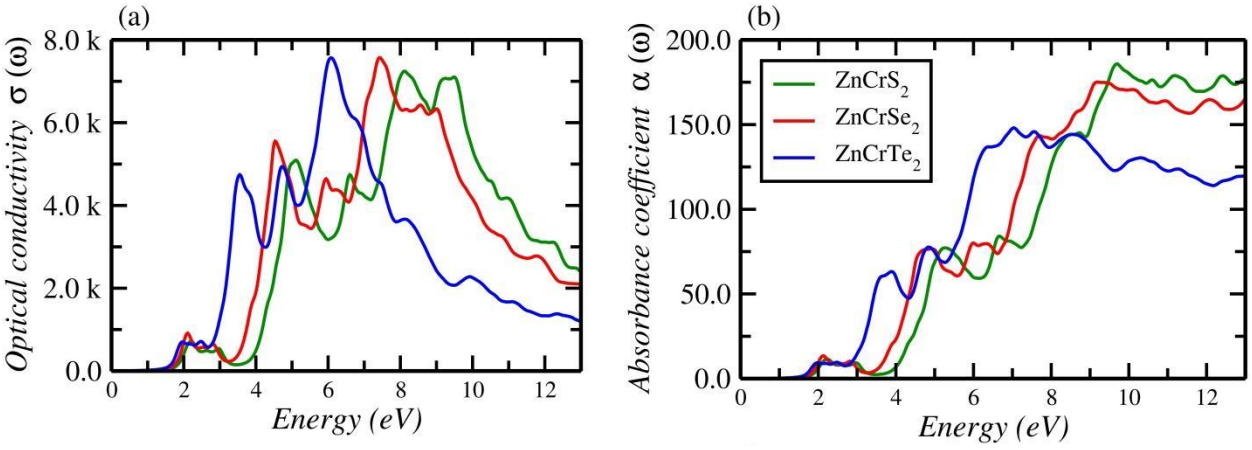

Fig. 7. **(a)** Optical Conductivity $\sigma(\omega)$; **(b)** Absorbance coefficient $\alpha(\omega)$ as a function of the photon energy of compounds $ZnCrX_2$ (X= S, Se, Te) using mBJ potential

3.3.4 Reflectivity and energy losses:

For the construction of opto-electronic surfaces in a particular device, it is imperative to explore the behavior of the material by the phenomenon of light reflectivity R (ω) [56]. The computed reflectivity pattern for all studied compounds is plotted in Fig. 8(a). The static values of reflectivity R (0) are 0.14, 0.16, and 0.19, also observed is that the value of R (0) increases by varying anions from S →Se →Te. The refractive index and reflectivity follow similar trends [51]. The maximum reflection is 47% for $ZnCrTe_2$ as its absorbance is lower than the other two compounds in the ultraviolet energy region and $ZnCrS_2$ shows lower reflectivity. It can be seen that $ZnCrS_2$ shows maximum reflectivity at 5 eV. Therefore, it can be confirmed from this research that material $ZnCrTe_2$ has a large reflection.

As we have observed, heating, dispersion, or scattering phenomena are some factors of optical loss that result in the energy loss of our studied compound $ZnCrX_2$ (X= S Se Te) as

shown in Fig. 8(b). Interband transitions, intraband transitions & plasmonic excitation, these important factors are provided by the spectra of energy loss. As a result, the electron energy loss spectrums with higher values provide information about plasmon resonance, also known as plasmon frequency. Incident radiation reflection off the material from its surface will occur in that specific range [53]. By adopting this equation: $(\omega) = \frac{\varepsilon_2(\omega)}{\varepsilon_1^2(\omega)+\varepsilon_2^2(\omega)}$, we can evaluate the energy loss L (ω) of any type of material [53]. Therefore, the loss parameters were evaluated for the optical behavior of the compounds, results show that they have maximum absorption and the low energy range lies from 0-8 eV minimum energy loss. Whereas in the high energy range (8-12 eV) for $ZnCrS_2$, the compound exhibits higher energy losses but absorbance is lower.

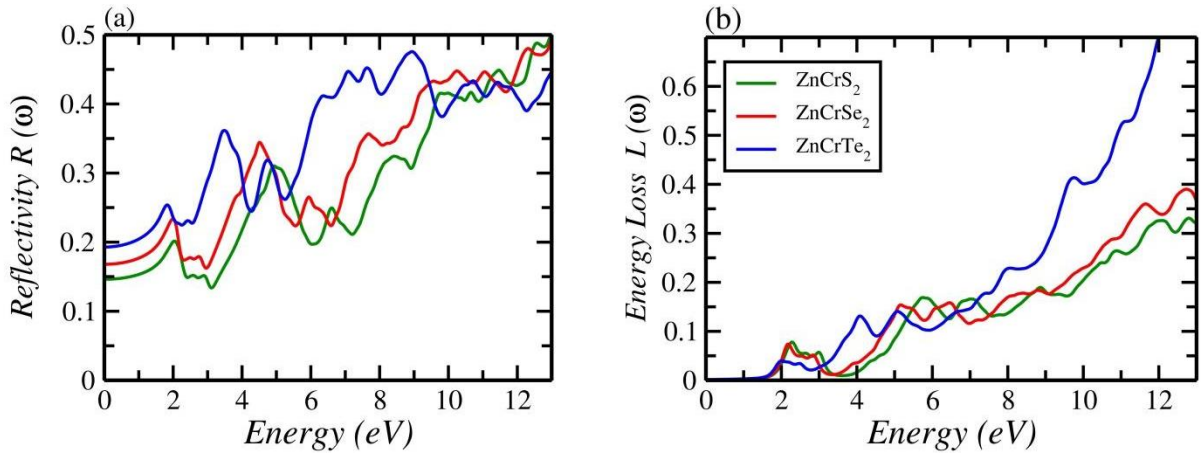

Fig.8 **(a)** Reflectivity R(ω), (b) Energy loss $L(\omega)$ as a function of the photon energy of compounds $ZnCrX_2$ (X= S, Se, Te) using mBJ potential

3.6 Thermoelectric performance:

During this technological age heat loss is higher; in this regard, researchers are considering converting the wasted heat into electrical energy [61, 62]. It is important to determine the thermoelectric behavior of compounds, thus the classical Boltzmann transport theory was implemented in the BoltzTraP code along with wien2k by using the following relation [61]**:**

$$\sigma_{\alpha\beta}(\varepsilon) = \frac{1}{N}\sum_{i,k} \quad \sigma_{\alpha\beta}(i,k)\frac{\delta(\varepsilon-\varepsilon_{i,k})}{\delta(\varepsilon)} \tag{8}$$

$$\sigma_{\alpha\beta}(i,\vec{k}) = e^2\tau_i v_\alpha(i,\vec{k})v_\beta(i,\vec{k}) \tag{9}$$

Equation 8 represents the transport coefficient and equation 9 is k points dependent transport tensor, also τ is relaxation time and $v_\alpha(i,\vec{k})$ is the group velocity component. In investigating transport properties no material is affected by band structure because electrons are the carriers of properties [56]. The performance of thermoelectric devices is calculated by using a dimensionless quantity, the figure of merits $ZT = \frac{S^2\sigma T}{k}$. In this equation, σ represents electrical conductivity, S represents the Seebeck coefficient, T represents temperature and k represents thermal conductivity. For an efficient thermoelectric device electrical conductivity and Seebeck coefficient value should be high and thermal conductivity must be low [63]**.** Chalcopyrites are considered to be valuable candidates for thermoelectric devices as they show low thermal conductivity and a high Seebeck coefficient. The thermoelectric behavior of the materials $ZnCrX_2$ (X = S, Se, Te) are shown in Fig. 9(a–d) and were investigated in the 0–800 K temperature range.

Fig. 9a shows the electrical conductivity that represents the availability of electrons for conduction by increment in temperature [60]. Taking integration of the transport tensor the σ as a function of absolute temperature and chemical potential are illustrated by equation [61] [64]:$\sigma_{\alpha\beta}(\alpha,\mu) = \frac{1}{\Omega}\int \quad \sigma_{\alpha\beta}(\varepsilon)\left[-\frac{\partial f_0(T,\varepsilon,\mu)}{\partial\varepsilon}\right]d\varepsilon$. Electrical conductivity presented 9a is calculated in exa (E) prefix. It is obvious from Fig. 9a that electrical conductivity also rises with an enhancement of temperature. It can be seen that at room temperature $ZnCrTe_2$ has higher electrical conductivity as compared to $ZnCrS_2$ and $ZnCrSe_2$. The electrical conductivity of $ZnCrTe_2$ at 300 K is $3 \times 10^{18}\, 1/\,\Omega.m$.

In thermoelectric properties, thermal conductivity is important to discuss. In semiconductors thermal conductivity is contributed by both electron and lattice vibrations and expressed by the relation $k = k_{lat} + k_{el}$, here k_{lat} is the lattice conductivity and k_{el} is electrical conductivity [65]. As the lattice conductivity contributes less to the thermal conductivity, only the electronic component is taken into account and it can be determined as: $k_e = \frac{1}{e^2T}\int \quad (\varepsilon-\mu)^2\,\sigma(\varepsilon)\frac{\partial f(\varepsilon)}{\partial\varepsilon}d\varepsilon$. It is assumed that thermal conductivities only depend on temperature, which is widely used in thermoelectric materials. Fig. 9b is the presentation of thermal conductivity that increases with an increment in temperature. At room temperature $ZnCrTe_2$

thermal conductivity is less than electrical conductivity but has a greater value of 70 T (W/m.k) than the other two compounds.

The Seebeck effect is defined by the potential created in a material by the movement of electrons, which results in a temperature difference across the material. The formula of the Seebeck coefficient in form of a distribution function is written as [62]:

$$S_{\alpha\beta}(T,\mu) = \frac{1}{eT\Omega\sigma_{\alpha\beta}(T,\mu)}\int \sigma_{\alpha\beta}(\varepsilon)(\varepsilon-\mu)\left[-\frac{\partial f_0(T,\varepsilon,\mu)}{\partial\varepsilon}\right]d\varepsilon$$

By changing the temperature, the Seebeck coefficient (*S*) values also change as shown in Fig. 9c. It is clear that the Seebeck coefficient is increasing at first and then decreasing after room temperature for $ZnCrSe_2$ and $ZnCrTe_2$ while for $ZnCrS_2$ the Seebeck value is lower than the other two compounds. Seebeck is calculated in micro (μ V/K) and the highest Seebeck value at 170 K is 260 μ V/K for $ZnCrTe_2$ which shifted to lower at room temperature. For $ZnCrSe_2$ the highest Seebeck value is 240 μ V/K at 390 K. The positive or negative sign of the Seebeck coefficient reveals the type of free charge carrier in the material. The positive Seebeck coefficient value possesses the p-type material and has extra holes while the negative Seebeck coefficient value possesses n-type material with the majority of electrons [51, 66]. It clarifies that all concerning materials are p-type materials with positive Seebeck coefficient values.

To predict the efficiency of material, it is important to know the power generation of material and this is known as the power factor of the material. The material will not be beneficial enough if its power factor is low while the best recommendation for material application is those that exhibit a higher power factor. It is related to the Seebeck coefficient and electrical conductivity so by attaining moderate *S* and σ values an optimal power factor can be achieved [67]. Depending on the temperature, the power factor is increasing as plotted in Fig. 9d. The power factor is plotted in Giga (G W/mk^{2}s) and PF value is maximum for $ZnCrTe_2$ at 500 K but decreases at 800 K. This means that $ZnCrTe_2$ has maximum power conversion efficiency.

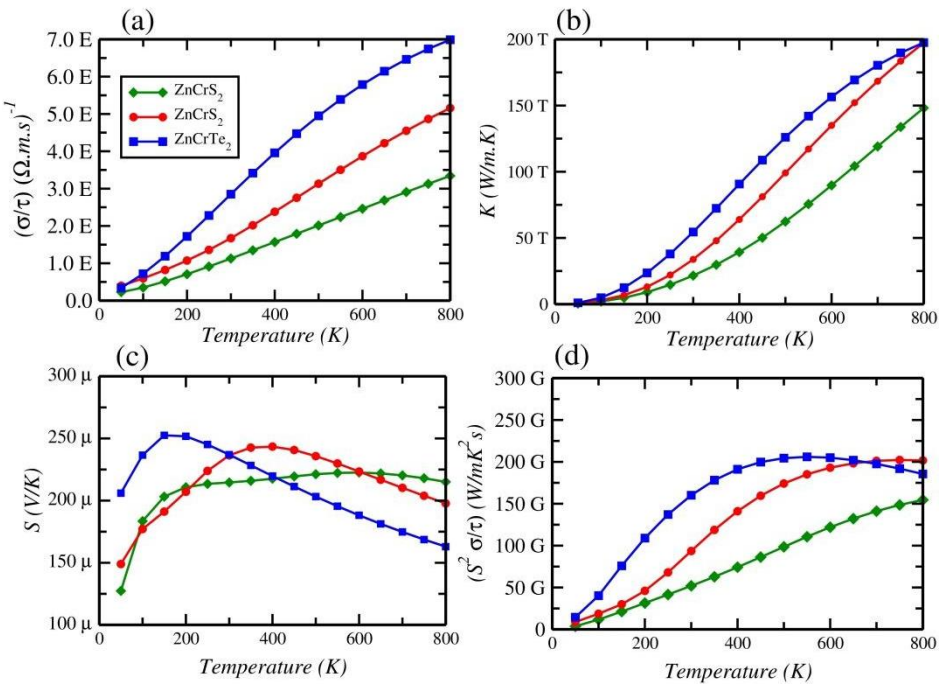

Fig. 9. (a) Electrical conductivities (σ); (b) Thermal conductivities (κ); (c) Seebeck coefficient (S); and (d) Power Factor (PF) for $ZnCrX_2$ (X= S, Se, Te) compounds using mBJ potential + BoltzTrap code

The figure of merits describes how far the concerning material is efficient for thermoelectric application. Depending on the temperature the figure of merits is presented in Fig. 10. It is found that ZT increases by increment in temperature. Figure 10 shows that $ZnCrTe_2$ is highly efficient as its figure of merit is high at 93% efficiency, while $ZnCrS_2$ is less efficient than the other two compounds. $ZnCrSe_2$ shows its maximum figure of merit at 400 K after that it goes on decreasing by increment in temperature. Calculated values of the figure of merit at different temperatures are presented in Table 2. Results reveal that $ZnCrTe_2$ has a maximum figure of merits up to 0.92 at 150 K which is greater than $CuInTe_2$ in bulk and surface [68]. It has been concluded that $ZnCrTe_2$ has credibility for thermoelectric applications like thermocouple, refrigerators, electric generators, etc., [69].

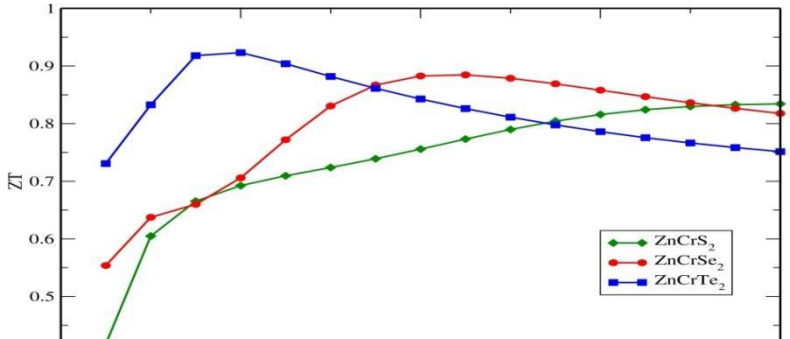

Fig. 10: Figure of merits of $ZnCrX_2$ (X=S, Se, Te) for $ZnCrX_2$ (X= S, Se, Te) compounds using mBJ potential + BoltzTrap code

Table 2: At different temperature figures of merit ZT for $ZnCrX_2$(X=S, Se, Te) compounds

Temperature	Compounds		
	$ZnCrS_2$	**$ZnCrSe_2$**	**$ZnCrTe_2$**
100 K	0.60	0.63	0.83
300 K	0.72	0.83	0.88
500 K	0.78	0.87	0.81
Max. figure of merits	0.83	0.88	0.92

4. Conclusion:

The present study shows the investigation of optoelectronic and thermoelectric properties of $ZnCrX_2$ (X= S, Se, Te) with first-principles calculations in the framework of DFT using WIEN2k code. The g round state energy of the compounds were calculated in I-42d space group, and they exhibit body centered tetragonal geometry with anion displacement toward the Cr atom. For the electronic properties using modified Becke-Johnson potential, the band gap tends to decrease in the order (S→ Se → Te) with 1.76 eV, 1.68 eV, and 1.59 eV values and chemical bonding is more ionic in $ZnCrS_2$ due to large electronegativity difference. From the optical properties, it is concluded that $ZnCrTe_2$ exhibits good optical conductivity and very small energy loss in the 0-6 eV energy range of the electromagnetic spectrum. The optical behavior of $ZnCrTe_2$ material makes it a promising candidate for optoelectronic devices. Plasmonic excitation is increased for $ZnCrTe_2$ after 6 eV causing more energy losses. In the high ultraviolet region absorbance is lower for $ZnCrTe_2$ while reflectivity is higher but in a lower region of the energy spectrum absorbance is higher which is suitable for photovoltaic applications. Moreover, $ZnCrSe_2$ and $ZnCrTe_2$ are characterized as highly efficient thermoelectric materials due to their lower thermal conductivity and high Seebeck coefficient

values. $ZnCrTe_2$ has maximum efficiency as it has 0.92 figures of merit. These compounds will provide an important perspective in the thermoelectric and optoelectronic fields.

5. Reference

[1] M. Magesh, A. Arun kumar, P. Vijayakumar, G. Anandha Babu, P. RamasamyOpt. Laser Technol., 56 (2014), 177

[2] Kerroum, D., H. Bouafia, B. Sahli, S. Hiadsi, B. Abidri, A. Bouaza, and M. A. Timaoui. *Optik* 139 (2017): 315-327.

[3] Cortés-Estrada, César Eduardo, César Ramírez-Márquez, et. al.*Chemical Engineering and Processing-Process Intensification* 183 (2023): 109237.

[4] Ranjan, Prabhat, and Tanmoy Chakraborty. *Materials Science in Semiconductor Processing* 127 (2021): 105745.

[5] Ranjan, Prabhat, Pancham Kumar, Tanmoy Chakraborty et. al. *Materials Chemistry and Physics* 241 (2020): 122346.

[6] Elalfy, Loay, Denis Music, and Ming Hu. *Physical Review B* 103 (2021): 075203.

[7] Nayebi, Payman, Kavoos Mirabbaszadeh, and Mahnaz Shamshirsaz., *Physica B: Condensed Matter* 416 (2013): 55-63.

[8] Murty, Y. Satyanarayana, S. Uthanna, B. Srinivasulu Naidu, and P. Jayarama Reddy., *Solid state communications* 79 (1991): 277-279.

[9] Ranjan, Prabhat, Pancham Kumar, Praveen K. Surolia, and Tanmoy Chakraborty. *Thin Solid Films* 717 (2021): 138469.

[10] Mishra, S., and B. Ganguli. *Solid state communications* 151 (2011): 523-528.

[11] Ghazal, I., H. Absike, A. Rachadi, and H. Ez-Zahraouy. *Optik* 260 (2022): 169077.

[12] Kushwaha, A. K., C-G. Ma, M. G. Brik, S. Bin Omran, and R. Khenata. *Materials Chemistry and Physics* 227 (2019): 324-331.

[13] Conejeros, Sergio, Pere Alemany, Miquel Llunell, Iberio de PR Moreira et. al., *Inorganic chemistry* 54, (2015): 4840-4849.

[14] Tabti, M., B. Doumi, A. Mokaddem, A. Boudali, M. D. Khodja, A. Bentayeb, and H. Moujri. *Acta Physica Polonica, A.* 136, (2019).

[15] Sadhukhan, Surasree, Banasree Sadhukhan, and Sudipta Kanungo. *Physical Review B* 106 (2022): 125112.

[16] Sadhukhan, Banasree, Yang Zhang, Rajyavardhan Ray, and Jeroen van den Brink. " *Physical Review Materials* 4 (2020): 064602.

[17] R. Terki, H. Feraoun, G. Bertrand, H. Aourag, Full potential linearized augmented plane wave investigations of structural and electronic properties of pyrochlore systems, J. Appl. Phys. 96 (2004) 6482

[18] Blaha, Peter, Karlheinz Schwarz, Georg KH Madsen, Dieter Kvasnicka, Joachim Luitz. "wien2k." An augmented plane wave+ local orbitals program for calculating crystal properties 60 (2001)

[19] P. Blaha, K. Schwarz, F. Tran, R. Laskowski, G.K.H. Madsen, L.D. Marks, WIEN2k: An APW+lo program for calculating the properties of solids, J. Chem. Phys. 152 (2020)

[20] Perdew, J. P. "Orbital functional for exchange and correlation: self-interaction correction to the local density approximation." *chemical physics letters* 64, (1979): 127-130.

[21] Jiang, Hong. *Journal of chemical physics* 138, (2013): 134115.

[22] Monkhorst, Hendrik J., and James D. Pack. "Special points for Brillouin-zone integrations." *Physical review B* 13, no. 12 (1976): 5188.

[23] Bennacer, Hamza, Abdelkader Boukortt, Said Meskine, Moufdi Hadjab, Mohamed Issam Ziane, and Ali Zaoui. *Optik* 159 (2018): 229-244.

[24] Becke, Axel D., and Marc R. Roussel. *Physical Review A* 39, (1989): 3761.

[25] Tran, Fabien, and Peter Blaha. *Physical review letters* 102, (2009): 226401.

[26] Hadjab, Moufdi, Smail Berrah, Hamza Abid, Mohamed Issam Ziane, Hamza Bennacer, and Ali H. Reshak. *Materials Chemistry and Physics* 182 (2016): 182-189.

[27] Sahin, S., Y. O. Ciftci, K. Colakoglu, and N. Korozlu. *Journal of alloys and compounds* 529 (2012): 1-7.

[28] Murnaghan, Francis Dominic. *Proceedings of the National Academy of Sciences* 30, (1944): 244-247.

[29] Mahdjoubi, R., Y. Megdoud, L. Tairi, H. Meradji, Z. Chouahda, S. Ghemid, and F. El Haj Hassan. *International Journal of Modern Physics B* 33, (2019): 1950045.

[30] Morsli, S., Caid, M., Rached, D., Rached, H., Benkhettou, N., & Bourachid, I. "Computational Condensed Matter", 27, (2021) e00550.

[31] Belhadj, M., A. Tadjer, B. Abbar, Z. Bousahla, B. Bouhafs, and H. Aourag. "physica status solidi (b)" 241, (2004): 2516-2528.

[32] Shi, Liwei, Jing Hu, Yun Qin, Yifeng Duan, Ling Wu, Xianqing Yang, and Gang Tang. "Journal of alloys and compounds" 611 (2014): 210-218.

[33] Vijaya lakshmi, D., and G. Kalpana. *physica status solidi (b)* 253, (2016): 1576-1584.

[34] Ketfi, Mohammed Elamin, Hamza Bennacer, Saber Saad Essaoud, Mohamed Issam Ziane, and Abdelkader Boukortt. *Materials Chemistry and Physics* 277 (2022): 125553.

[35] Salehi, H., and E. Gordanian. *Materials Science in Semiconductor Processing* 47 (2016): 51-56.

[36] Zhang, R. Q., C. S. Lee, and S. T. Lee. *The Journal of Chemical Physics* 112, (2000): 8614-8620.

[37] Bikerouin, M., M. Balli, J. D. Correa, and M. E. Mora-Ramos. *Current Applied Physics* 32 (2021): 11-23.

[38] Shah Fahad , G. Murtaza , T. Ouahrani, R. Khenata, Masood Yousaf, S.Bin Omran , Saleh Mohammad, Journal of Alloys and Compounds 646 (2015) 211e222

[39] Rizwan, Muhammad, Z. Khadija, Tariq Mahmood, S. S. A. Gillani, and Muhammad Isa Khan. *Physica B: Condensed Matter* 602 (2021): 412553.

[40] Kumar, V., and S. K. Tripathy. *Journal of alloys and compounds* 582 (2014): 101-107.

[41] Asadullayeva, Saida G., Narmin A. Ismayilova, and Qurban Y. Eyyubov. *Solid State Communications* 356 (2022): 114950.

[42] Fahad, Shah, G. Murtaza, T. Ouahrani, R. Khenata, Masood Yousaf, S. Bin Omran, and Saleh Mohammad. *Journal of Alloys and Compounds* 646 (2015): 211-222.

[43] Huma, Muniba, Muhammad Rashid, Q. Mahmood, Eman Algrafy, Nessrin A. Kattan, A. Laref, A. S. Bhatti, *Mater. Sci. Semiconductor Process.* 121 (2021) 105313

[44] Kumari, J., C. Singh, B. L. Choudhary, and A. S. Verma. *Physics and Chemistry of Solid State* 23, (2022): 728-740.

[45] Verma, Pallavi, Chandravir Singh, Peeyush Kumar Kamlesh, Kulwinder Kaur, and Ajay Singh Verma. *Journal of Molecular Modeling* 29, no. 1 (2023): 23.

[46] Xue, Suqin, Jing Ning, Bohang Zhang, Qiao Wu, Fuchun Zhang, and Weibin Zhang. *Coatings* 12, (2022): 1778.

[47] Ismail, Khawar, G. Murtaza, Shaista Tahir, Ghazanfar Nazir, Nessrin A. Kattan, Hind Albalawi, Bakhtiar Ul Haq, and Manal Morsi. *Journal of Solid State Chemistry* 314 (2022): 123432.

[48] Hassan, M., N. A. Noor, Q. Mahmood, and B. Amin. *Current Applied Physics* 16, (2016): 1473-1483.

[49] Ulian, Gianfranco, Daniele Moro, and Giovanni Valdrè. *Data in brief* 32 (2020): 106208.

[50] Bennacer, Hamza, Smail Berrah, Abdelkader Boukortt, and Mohamed Issam Ziane. "Electronic and optical properties of GaInX 2 (X= As, P) from first principles study." (2015)

[51] Yaqoob, N., B. Sabir, G. Murtaza, Rana M. Arif Khalil, Nawaz Muhammad, and A. Laref. *Physica B: Condensed Matter* 574 (2019): 311656.

[52] Bendjemai, M., H. Bouafia, B. Sahli, A. Dorbane, Ş. Uğur, G. Uğur, and S. Mokrane. *Physica B: Condensed Matter* 599 (2020): 412463.

[53] Benaadad, Merieme, Abdelhakim Nafidi, Samir Melkoud, Issam Mahraj, and Mariyam Salmi.." *Physica B: Condensed Matter* 642 (2022): 414118.

[54] Benlamari, S., H. Meradji, and S. Ghemid. "First-principle study of structural and optical properties of MgSiSb2." (2018).

[55] Ciftci, Y. O., and I. O. Alp. *Materials Today Communications* 24 (2020): 101263.

[56] Murtaza, G., and Hafiz Hamid Raza. *Optical and Quantum Electronics* 52, (2020): 1-21.

[57] Thahirunnisa, S. R., IB Shameem Banu, M. Mohamed Sheik Sirajuddeen, and IkramUn Nabi Lone.." *Computational Condensed Matter* 29 (2021): e00601.

[58] Sharma, Sheetal, and Ajay Singh Verma*The European Physical Journal B* 87, (2014): 1-14.

[59] Bekhedda, Kheira, Said Hiadsi, Mohamed Issam Ziane, and Kaci Samira. *Russian Journal of Physical Chemistry A* 96, (2022): 1986-1994.

[60] Yaseen, Muhammad Shahzad, G. Murtaza, and R. M. Arif Khalil. *Optical and Quantum Electronics* 51, (2019): 1-14.

[61] Yaseen, M. S., G. Murtaza, and Rana M. Arif Khalil. *Current Applied Physics* 18, (2018): 1113-1121.

[62] Tab, Slimane, Abdelkader Boudali, Mohamed Berber, Mohamed Driss khodja, Omari Lhaj El Hachemi, and Hayat Moujri. *Applied Physics A* 126 (2020): 1-10.

[63] Abdel-Motaleb, Ibrahim M., and Syed M. Qadri.." *arXiv preprint arXiv:1704* (2017).*07742*

[64] Mahmood, Q., M. Yaseen, Bakhtiar Ul Haq, A. Laref, and Aalia Nazir. *Chemical Physics* 524 (2019): 106-112.

[65] Khan, Sajid, R. Neffati, Tariq Usman, Muhammad Waqar Ahsraf, Shamim Khan, and G. Murtaza. *Journal of Rare Earths* (2022).

[66] D. Vasileska, H.R. Khan, S.S. Ahmed, G. Kannan, C. Ringhofer Nano-Electronic Devices, Springer, 2011, 97–181.

[67] Prakash Govindaraj , Kowsalya Murugan , Kathirvel Venugopal, Materials Chemistry and Physics 295 (2023) 127190

[68] Rai, D. P., A. Shankar, Anup Pradhan Sakhya, T. P. Sinha, P. Grima-Gallardo, H. Cabrera, R. Khenata, Madhav Prasad Ghimire, and R. K. Thapa. *Journal of Alloys and Compounds* 699 (2017): 1003-1011.

[69] V. Petrov, et al., Appl. Phys. B Laser Optic. 78 (2004) 543.